NASA CONTRACTOR REPORT

NASA CR-2689

NASA CR-2

FUNDAMENTAL ANALYSIS OF THE FAILURE OF POLYMER-BASED FIBER REINFORCED COMPOSITES

M. F. Kanninen, E. F. Rybicki,
W. I. Griffith, and D. Broek

Prepared by
BATTELLE, COLUMBUS LABORATORIES
Columbus, Ohio 43201
for Ames Research Center

NATIONAL AERONAUTICS AND SPACE ADMINISTRATION • WASHINGTON, D. C. • APRIL 1976

1. Report No.	2. Government Accession No.	3. Recipient's Catalog No.
CR-2689		

4. Title and Subtitle	5. Report Date
"Fundamental Analysis of the Failure of Polymer-Based Fiber Reinforced Composites"	April 1976
	6. Performing Organization Code
7. Author(s)	8. Performing Organization Report No.
M.F. Kanninen, E.F. Rybicki, W.I. Griffith, and D. Broek	
	10. Work Unit No.
9. Performing Organization Name and Address	11. Contract or Grant No.
Battelle, Columbus Laboratories 505 King Avenue Columbus, Ohio 43201	NSG-2038
	13. Type of Report and Period Covered
12. Sponsoring Agency Name and Address	Contractor Report/Final Report
National Aeronautics & Space Administration Washington, D.C. 20546	14. Sponsoring Agency Code

15. Supplementary Notes

16. Abstract

A mathematical model is being developed that will permit predictions of the strength of fiber reinforced composites containing known flaws to be made from the basic properties of their constituents. The approach is to embed a local heterogeneous region (LHR) surrounding the crack tip into an anisotropic elastic continuum. The intent is to have the model (1) permit an explicit analysis of the micromechanical processes involved in the fracture process, and (2) remain simple enough to be useful in practical computations. Material properties used in the analysis are to be obtained from a concurrent experimental program being carried out at Virginia Polytechnic Institute and State University.

Computations for arbitrary flaw size and orientation under arbitrary applied load combinations have been performed for unidirectional composites with linear elastic-brittle constituent behavior. The mechanical properties were nominally those of graphite epoxy. With the rupture properties arbitrarily varied to test the capability of the model to reflect real fracture modes in fiber composites, it is shown in the report that fiber breakage, matrix crazing, crack bridging, matrix-fiber debonding, and axial splitting can all occur during a period of (gradually) increasing load prior to catastrophic fracture. Of most importance, the computations reveal qualitatively the sequential nature of the stable crack growth process that precedes fracture in composites. Quantitative comparisons with the VPISU experimental results on edge-notched unidirectional graphite epoxy specimens have also been made and were found to be in fair agreement.

17. Key Words (Suggested by Author(s))	18. Distribution Statement
fiber reinforced composites failure modes fracture micromechanical failure analysis micromechanical fracture mechanics microstructural failure	UNCLASSIFIED-UNLIMITED STAR Category 24

19. Security Classif. (of this report)	20. Security Classif. (of this page)	21. No. of Pages	22. Price*
UNCLASSIFIED	UNCLASSIFIED	45	$3.25

For sale by the National Technical Information Service, Springfield, Virginia 22161

TABLE OF CONTENTS

LIST OF TABLES

LIST OF FIGURES

FUNDAMENTAL ANALYSIS OF THE FAILURE OF POLYMER-BASED FIBER REINFORCED COMPOSITES

INTRODUCTION

There are many different ways in which a structure made of a fiber reinforced composite material can become unable to adequately perform its primary function. In each such instance failure is considered to have occurred. The possible failure modes therefore encompass a wide range of possibilities from simple loss of structural rigidity due to gross inelastic deformation (e.g., yielding), through a reduction in load-carrying capacity due to localized damage or separation (e.g., interply delamination), to the complete loss of strength due to large-scale crack growth and fracture. Each of these failure modes can be gradual or rapid depending on the nature of the applied loads, the material properties, the geometry of the structure, and the presence of cracks or flaws. For polymer-based composites, the loading rate, the temperature, and previous load history can also play prominent roles.

In the work described in this report, emphasis is placed upon fracture and, therefore, the work will be primarily concerned with the "strength" of fiber composites containing known flaws. The term strength is conventionally taken to mean the load level at which failure occurs in a standard test specimen. Clearly, the strength will be a function of many different parameters arising in the test program and may or may not be directly applicable to engineering design situations. The primary purpose of the research described in this report is to provide a bridge between standard laboratory test procedures and actual engineering applications of fiber composites that will allow accurate reliable estimates of the failure loads for aircraft and other engineering structures. Such a capability does not presently exist.

The design tool that should be developed for the safe and efficient utilization of composite materials is a predictive capability for fracture that can take account of the applied loading, the geometry of the structure, and the environmental effects in terms of readily measurable properties of the composite's constituents and of its microstructural design. The primary benefits accruing from such an analytical capability are twofold. First, for a given structure, material, and load, the critical flaw size and type in a structural component can be estimated for comparison with actual flaws observed in an inspection program. Second, guidelines can be provided for the designer to tailor more fracture resistant "tougher" materials for specific engineering applications.

PROGRAM PLAN AND SUMMARY OF PROGRESS

The work described in this report represents the first year of effort in what is planned as a multiyear program. The specific objective of the first year's work was to develop the basic mathematical procedures required for the analysis model. To implement this work, attention was focussed on unidirectional composites with linear elastic-brittle material behavior. In subsequent work, the model will be extended to treat angle ply laminates and will include further refinements (e.g., inelastic constituent behavior) required in order to treat actual engineering problems.

The primary objective of the work will be achieved only if the mathematical model developed is capable of delineating the role of the various micromechanical failure processes that dictate the ultimate failure point of fiber reinforced composites. The research described in this report seeks this end by merging a micromechanical failure analysis with a macromechanical fracture mechanics approach. This approach treats the material as heterogeneous and anisotropic where microstructural effects predominate and as homogeneous and anisotropic where it is permissible and practical to do so. In this way, direct consideration can be given to

- The external size and shape of the structure and the laminate stacking sequence
- The applied loads acting on the structure, both mechanical and thermal, and environmental effects
- The size, shape, and orientation of a flaw in the laminate.

In particular, the manner in which these parameters influence the sequence of microstructural failure events whereby a flaw extends stably under an increasing load up to the point of catastrophic fracture will be determined. It should be understood that the conventional approach to fracture analysis, linear elastic fracture mechanics, is not capable of coping with this degree of complexity, thus necessitating the more general development being pursued here.

Linear elastic fracture mechanics (LEFM) is a predictive technique applicable to structural components containing crack-like flaws when the material used fits certain key assumptions used in the LEFM theory. Specifically, the material must behave very nearly as would a completely linear elastic perfectly homogeneous ideal material. The LEFM approach has been successful when properly applied (e.g., to high strength steel), but considerably less successful in applications where the basic assumptions are not well satisfied. Fiber reinforced composite materials are an outstanding example of the latter case. In particular, in fiber composites with a flaw, a nonlinear "damage" zone is generally produced at the flaw. This zone, generally growing in a stable manner under an increasing applied load, has a profound effect on the eventual point of complete fracture. This is shown, for example, in the work of Mandell, et al. [1]* as well as by many other investigators.

The damage zones in a fiber composite are the result of a large number of discrete failure processes, e.g., fiber breaking, matrix yielding, etc., that occur in the highly stressed region ahead of a crack-like flaw. These individual micromechanical events do not conform to the basic assumptions of LEFM. Consequently, it is not surprising that the agregate of such processes cannot be treated by LEFM. What is therefore needed is a generalized fracture mechanics treatment which explicitly recognizes the fundamental nature of damage growth in composite materials. Specifically, a proper analysis of fracture in fiber composites must be cognizant of two key features: the generally anisotropic constitutive behavior of the material, and the heterogeneous nature of the fracture process.

The approach developed in this report can be likened conceptually to boundary layer theory and, in application, to the well-established singular perturbation and matched asymptotic expansion techniques of fluid mechanics. That is, the problem of a composite material containing a flaw is divided into distinct "inner" and "outer" regions. In each of these regions, the material is modeled in different ways. The inner region, which contains the crack tip, is considered on the microscopic level and treats the material as being heterogeneous. The outer region surrounds the crack tip region. It is treated as a homogeneous orthotropic continuum. For simplicity, the inner crack tip region will be referred to in this report as the LHR (for local heterogeneous region) while the outer region will be simply called the continuum.

---

* References are given on page 45.

The LHR consists of elements representing the matrix, the fibers, and the fiber-matrix interface zones. The constitutive relations of these elements, up to and including their rupture points, are presumed to be known from experiments. Any element of a fiber composite ruptures when an intrinsic critical energy dissipation rate can be provided at some point of that element. These critical values are assumed to be independent of the local stress field environment at the point of incipient rupture. This permits data from fracture tests on isolated fibers, matrix material, and, possibly, unflawed composites (to obtain interface strengths) to be directly inserted into the model. Material properties used in the analysis work and, ultimately, critical tests of the predictions of the model will be obtained from a concurrent experimental program being carried out under NASA sponsorship at Virginia Polytechnic Institute and State University.

Progress to date has permitted computations to be performed for unidirectional composites with elastic-perfectly brittle constituent behavior. The mechanical properties have been those of graphite epoxy. The rupture properties have also been arbitrarily varied to test the capability of the model to reflect real fracture modes in fiber composites. It has been shown that fiber breakage, crack bridging, matrix-fiber debonding, and axial splitting can all occur during a period of (gradually) increasing load prior to catastrophic fracture. In this way, the sequential and interrelated manner in which each individual local rupture event occurs during damage growth preceding fracture in fiber composites is revealed by the computations.

DESCRIPTION OF THE ANALYSIS TECHNIQUE

In the preceding section of this report, the objectives of the work and an outline of the general approach were given. The focal point for this description was the two-dimensional local heterogeneous region (LHR) surrounding the crack tip. A typical LHR model is shown in Figure 1. Depicted is a unidirectional fiber composite containing three distinct components: the fibers, the matrix, and the fiber-matrix interface zones. In this section of the report, the discrete elements that comprise the LHR and the manner in which they are assembled to give a quantitative predictive capability for composite fracture will be described in detail.

LHR Boundary Conditions

In the work performed so far, the interaction between the LHR and the continuum, as is appropriate for preliminary stages of the work, has been taken in the simplest possible manner. This is by specifying the displacements on the boundary of the LHR in accord with the "rigid boundary conditions" approach. Use of this scheme is tantamount to assuming that the LHR is large enough that the nonlinear inhomogeneity of the crack tip region does not affect the periphery of this region. In other words, the LHR and the continuum are assumed to be uncoupled. Consequently, the displacements at the LHR boundary are exactly the same as if the entire cracked body is an elastic continuum. The required relations can therefore be obtained from the work of Sih and Liebowitz [2]. Their approach is briefly summarized, as follows.

Consider a plate with its major dimensions lying in the xy plane. For either plane stress or plane strain deformation, the inplane strains ε_x, ε_y, and γ_{xy} will depend only on the inplane stresses σ_x, σ_y, and τ_{xy}. Hence, the appropriate constitutive relations for a rectilinearly anisotropic body in a state of plane deformation are given by

$$\begin{aligned} \varepsilon_x &= a_{11}\sigma_x + a_{12}\sigma_y + a_{16}\tau_{xy} \\ \varepsilon_y &= a_{12}\sigma_x + a_{22}\sigma_y + a_{26}\tau_{xy} \\ \gamma_{xy} &= a_{16}\sigma_x + a_{26}\sigma_y + a_{66}\tau_{xy} \end{aligned} \qquad (1)$$

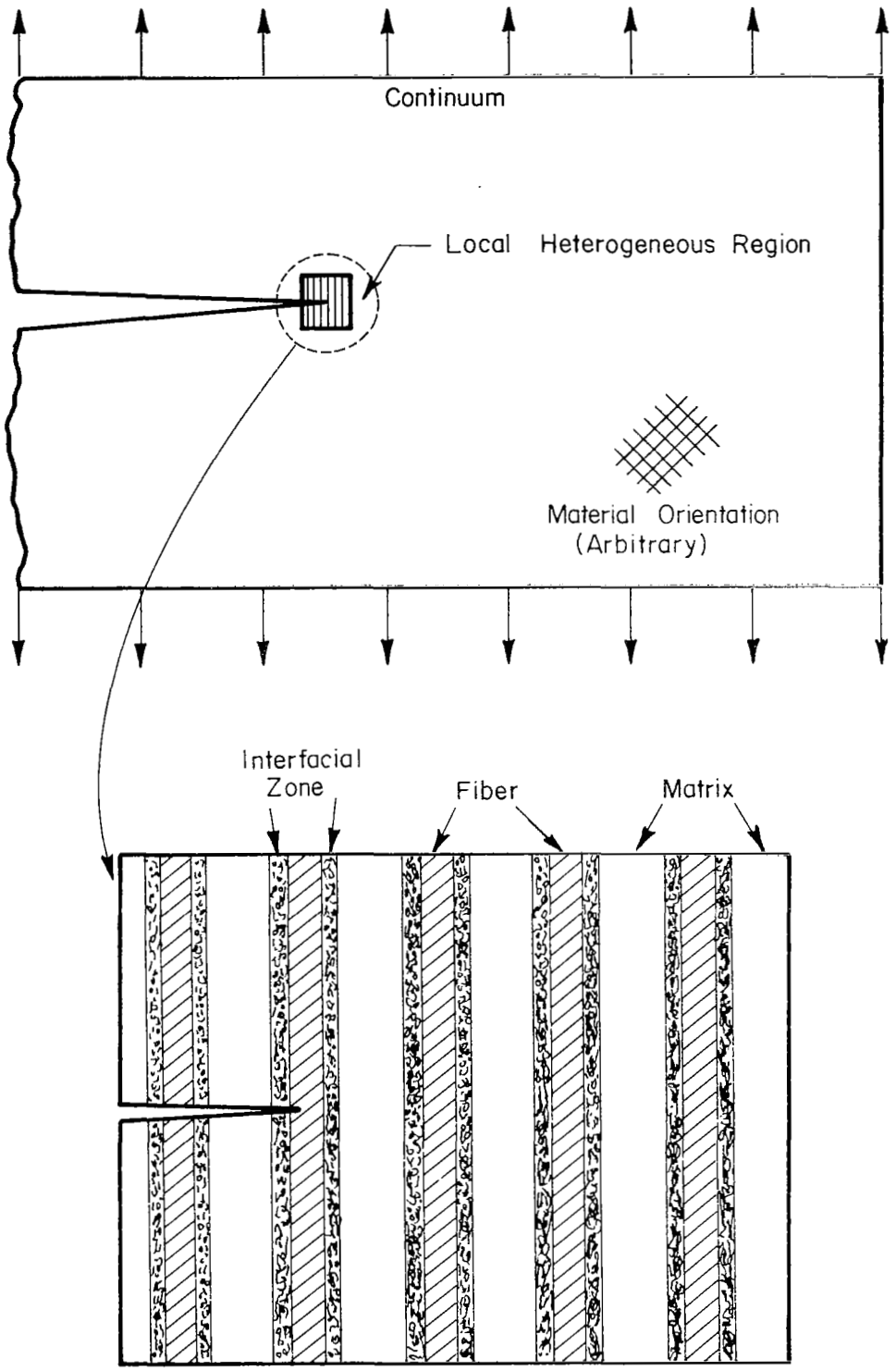

FIGURE 1. THE LHR CONCEPT

Sih and Liebowitz show that the solution to the governing differential equation of two-dimensional anisotropic elasticity theory is associated with the roots of the characteristic equation

$$a_{11}\,s^4 - 2a_{16}s^3 + (2a_{12} + a_{66})\,s^2 - 2\,a_{26}\,s + a_{22} = 0\ . \qquad (2)$$

It can be shown that the roots of Equation (2) are either complex or are pure imaginary. Hence, these can be labeled s_1, s_2, $\bar{s}_1$, and $\bar{s}_2$. This suggests the introduction of the complex variables $z_1 = x + s_1 y$ and $z_2 = x + s_2 y$. The plane problem of an anisotropic body is thereby reduced to the determination of two complex potential functions of a complex variable $\phi(z_1)$ and $\psi(z_2)$ that satisfy the prescribed boundary conditions of the problem.

As further shown in reference 2, the displacement field is expressed in terms of the potential functions by the relations

$$\begin{aligned} u &= 2\,Re\,\{p_1\,\phi(z_1) + p_2\,\psi(z_2)\} \\ v &= 2\,Re\,\{q_1\,\phi(z_1) + q_2\,\psi(z_2)\}\ , \end{aligned} \qquad (3)$$

where u and v are the x and y displacement components and

$$p_1 = a_{11}\,s_1^2 + a_{12} - a_{16}\,s_1 \quad , \quad p_2 = a_{11}\,s_2^2 + a_{12} - a_{16}\,s_2$$

$$q_1 = \frac{1}{s_1}\,(a_{12}\,s_1^2 + a_{22} - a_{26}\,s_1) \ , \quad q_2 = \frac{1}{s_2}\,(a_{12}\,s_2^2 + a_{22} - a_{26}\,s_2) \ .$$

Omitting the details, potential functions for a cracked body infinite in extent have been determined for insertion into Equations (3). In particular, a solution for remote loading consisting of a uniform tensile loading σ acting in the direction normal to the crack plane and a shear loading τ parallel to the crack

plane for a crack of length $2a$ can be obtained. For a polar coordinate system with origin at the crack tip as shown in Figure 2, the displacements near the crack tip are given by

$$u = K_I\left(\frac{2r}{\pi}\right)^{1/2} Re\left\{\frac{1}{s_2-s_1}\left[s_1 p_2 (\cos\phi + s_2 \sin\phi)^{1/2} + \right.\right.$$

$$\left.\left. - s_2 p_1 (\cos\phi + s_1 \sin\phi)^{1/2}\right]\right\} +$$

$$+ K_{II}\left(\frac{2r}{\pi}\right)^{1/2} Re\left\{\frac{1}{s_1-s_2}\left[p_2 (\cos\phi + s_2 \sin\phi)^{1/2} + \right.\right.$$

$$\left.\left. - p_1 (\cos\phi + s_1 \sin\phi)^{1/2}\right]\right\} \qquad (4)$$

and

$$v = K_I\left(\frac{2r}{\pi}\right)^{1/2} Re\left\{\frac{1}{s_1-s_2}\left[s_1 q_2 (\cos\phi + s_2 \sin\phi)^{1/2} + \right.\right.$$

$$\left.\left. - s_2 q_1 (\cos\phi + s_1 \sin\phi)^{1/2}\right]\right\} +$$

$$+ K_{II}\left(\frac{2r}{\pi}\right)^{1/2} Re\left\{\frac{1}{s_1-s_2}\left[q_2 (\cos\phi + s_2 \sin\phi)^{1/2} + \right.\right.$$

$$\left.\left. - q_1 (\cos\phi + s_1 \sin\phi)^{1/2}\right]\right\} \quad , \qquad (5)$$

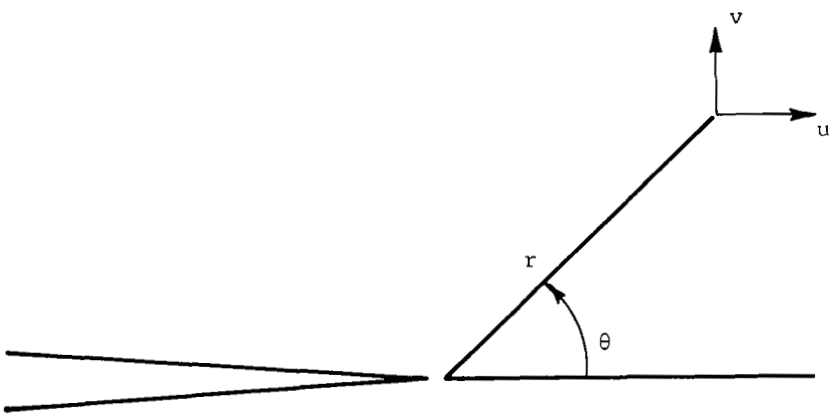

FIGURE 2. DISPLACEMENT COMPONENTS FOR A POINT IN THE VICINITY OF THE CRACK TIP

where

$$K_I = \sigma \sqrt{\pi a}$$

and (6)

$$K_{II} = \tau \sqrt{\pi a}$$

are the Mode I and Mode II stress-intensity factors for the problem.

Equations (4) and (5) can be used to determine displacements on the LHR boundary via the rigid boundary-condition approach. This means that the applied stresses acting on the body are transmitted through the continuum region to the crack-tip region and are "sensed" at the crack tip in terms of the stress-intensity factors K_I and K_{II}. An independent specification of the load and crack length is therefore unnecessary. Hence, although derived for an infinite medium, the approach can be used for bodies with finite boundaries by simply inserting the appropriate stress-intensity factors. In doing this, it must be tacitly assumed that the LHR is (1) large enough relative to the microstructural dimensions of the composite that the boundary displacements are closely given by continuum theory and (2) small enough relative to the crack length and dimensions of the body that the singular behavior of the continuum solution at the crack tip dominates.

While appropriate for preliminary work, it is anticipated that the rigid boundary condition approach--even with periodic updating to reflect the progress of the crack through the LHR--may prove to be too restrictive. Therefor, in subsequent work, a flexible boundary-condition approach which extends an approach developed in work previously carried out at Battelle [3] will be used. This is described in more detail in the Recommended Further Research section of this report. It might be noted that with flexible boundary conditions, crack length and load must be specified individually.

The LHR Element

As shown in Figure 1, the LHR for a fiber reinforced composite is considered to be made up of three different types of constituents: fiber, matrix, and fiber-matrix interface. Each of the individual constituents in the LHR must be capable of rupturing to allow the body to exhibit the changes in strength that correspond to various levels and orientations of local breakage. A good deal of success has been obtained by Kanninen [4,5] using "spring-like" elements to model a local fracture phenomena. This fact, taken together with the increased computational simplicity of this approach, has led to the adoption of the basic element shown in Figure 3 for this work.

As shown in Figure 3, each element has eight degrees of freedom and is connected in the LHR at its four corner node points. Extensional stiffness is provided by four extensional connectors. These connectors resemble simple extensional springs, but also have a lateral contraction or Poisson effect. A material made up of a set of these connectors behaves in uniform extension exactly like a homogeneous orthotropic material. Similarly, shear stiffness is incorporated in the element through a rotary spring at each node point to give the proper response to shear loadings. The values of the spring constants are functions of the material's elastic constants and of the element size and shape.

In addition to giving the proper response to loads, the LHR elements fracture according to the "codes" shown in Figure 4. In Figure 4, Fracture Code 1 represents an increment of crack extension in the plane lying midway between Nodes 1 and 4 that extends from the left side of the element to the center of the element. Fracture Code 2 represents the continuation of the crack to the right side of the element. Fracture Codes 3 and 4 represent similar increments of cracking in the vertical direction.

Using an energy approach, it is possible to trace those components of the elemental stiffness matrix that are associated with each fracture code in every element in the LHR. This information can be assembled into the stiffness matrix such that a solution can be obtained for the incipient rupture of any subelement in the LHR. Note that this is most easily possible if (as in the present work), the constituent behavior is restricted to being linear elastic to the rupture point. Inelastic behavior, while more complicated, is not precluded, however.

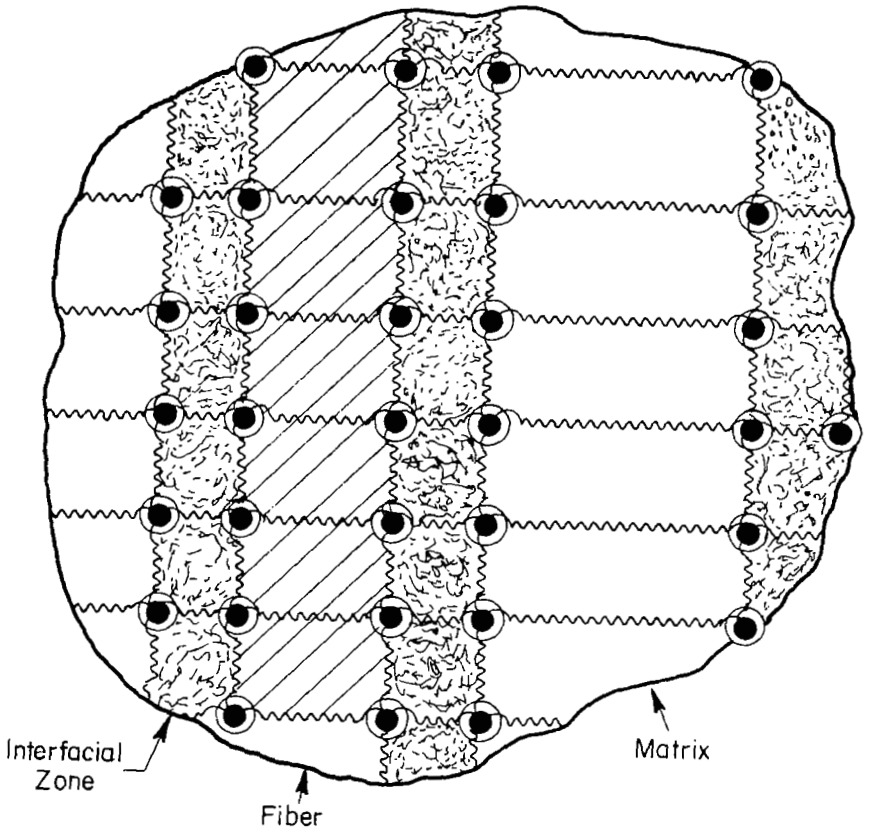

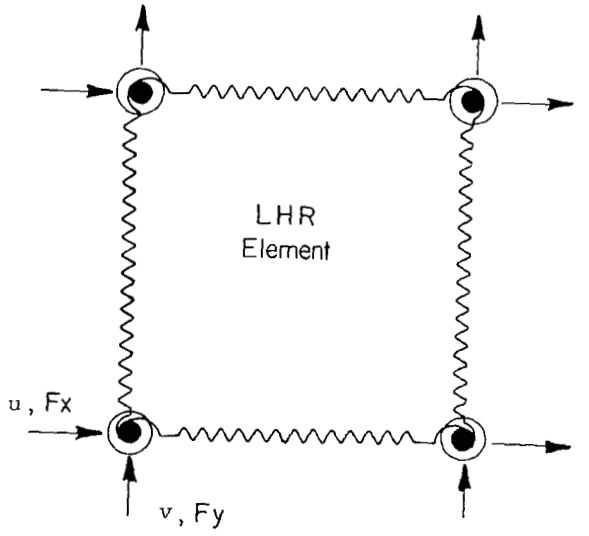

FIGURE 3. DETAILED REPRESENTATION OF AN LHR ELEMENT

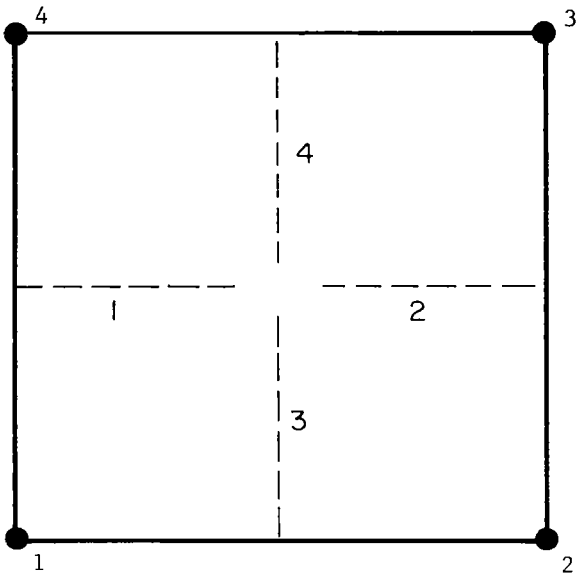

FIGURE 4. THE FRACTURE CODES CONTAINED IN AN LHR ELEMENT

Knowledge of the stiffness components attributable to each fracture condition also provides a method of calculating the energy-release rate for crack advance by any of the four codes provided for in each LHR element. Of course, the critical rupture energy values must be specified to provide a decision rule for breakage in each separate element. Note that while the model allows separate critical values to be specified for each of the four fracture codes for every one of the elements in the LHR, ordinarily different values will be specified only for the different constituents, i.e., fiber, matrix, or interface.

Elemental Stiffness Formulation

Energy principles can conveniently be used to determine the stiffness of the LHR structure. The sign conventions for an LHR element will be taken as shown in Figure 5. Then, using the following notation:

C_i = rotational spring constant at the $i^{\underline{th}}$ node

K_{xx}^{ij} = extensional stiffness in the x direction between the $i^{\underline{th}}$ and $j^{\underline{th}}$ nodes

K_{yy}^{ij} = extensional stiffness in the y direction between the $i^{\underline{th}}$ and $j^{\underline{th}}$ nodes

K_{xy}^{ij} = cross extensional component (effect of Poisson's ratio) between the $i^{\underline{th}}$ and $j^{\underline{th}}$ nodes

u_i = x displacement at the $i^{\underline{th}}$ node

v_i = y displacement at the $i^{\underline{th}}$ node,

the total strain energy U stored in the element for any set of arbitrary nodal displacements u_i and v_i can be written as

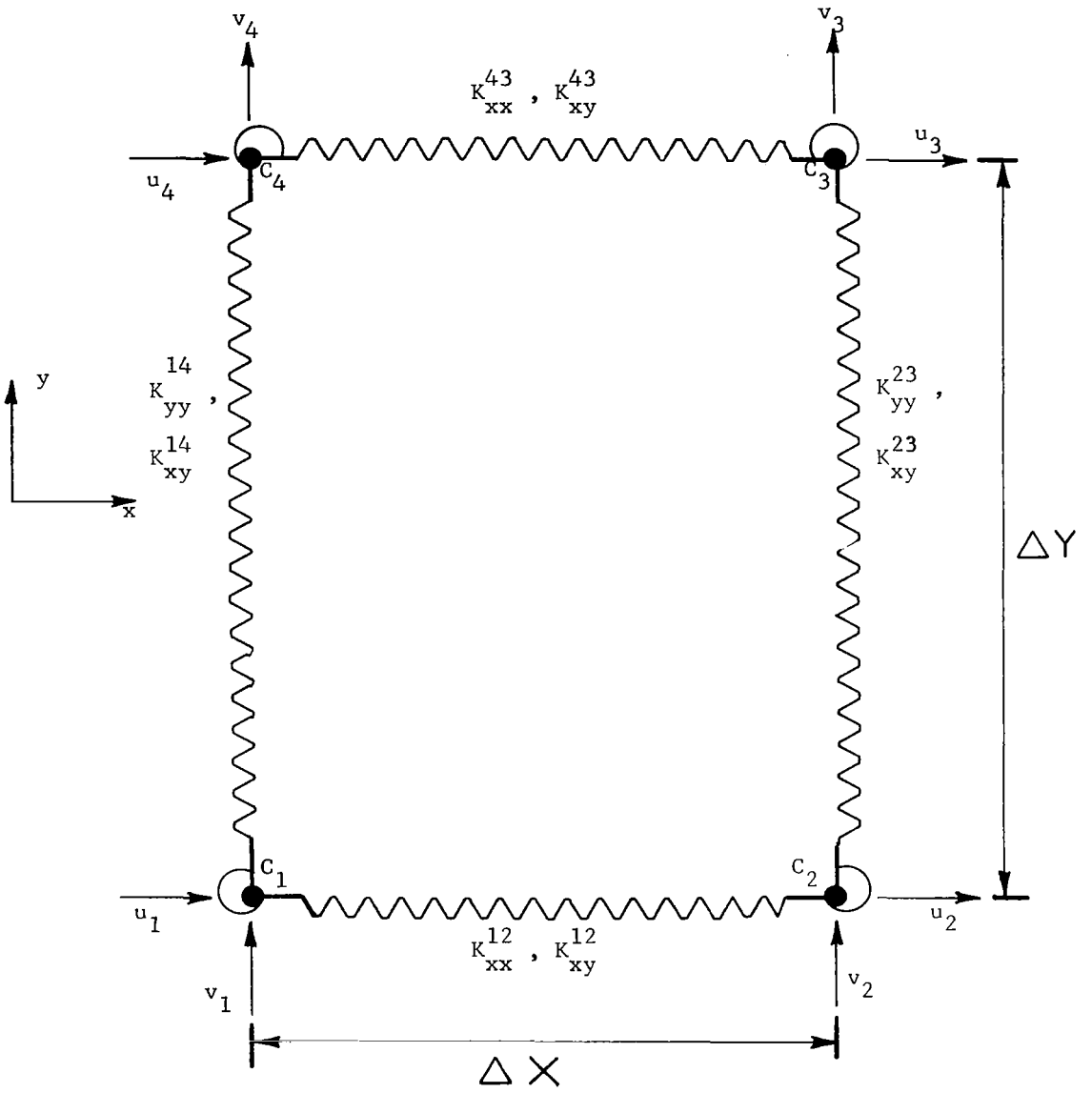

FIGURE 5. A TYPICAL LHR ELEMENT

$$U = \frac{1}{2} K_{xx}^{12} (u_2 - u_1)^2 + K_{xy}^{12} \left\{ \frac{v_4 - v_1}{2} + \frac{v_3 - v_2}{2} \right\} (u_2 - u_1)$$

$$+ \frac{1}{2} K_{xx}^{43} (u_3 - u_4)^2 + K_{xy}^{43} \left\{ \frac{v_4 - v_1}{2} + \frac{v_3 - v_2}{2} \right\} (u_3 - u_4)$$

$$+ \frac{1}{2} K_{yy}^{14} (v_4 - v_1)^2 + K_{xy}^{14} \left\{ \frac{u_3 - u_4}{2} + \frac{u_2 - u_1}{2} \right\} (v_4 - v_1)$$

$$+ \frac{1}{2} K_{yy}^{23} (v_3 - v_2)^2 + K_{xy}^{23} \left\{ \frac{u_3 - u_4}{2} + \frac{u_2 - u_1}{2} \right\} (v_3 - v_2)$$

$$+ \frac{1}{2} C_1 \left\{ \frac{(v_2 - v_1)}{\Delta x} + \frac{(u_4 - u_1)}{\Delta y} \right\}^2$$

$$+ \frac{1}{2} C_2 \left\{ \frac{(u_3 - u_2)}{\Delta y} + \frac{(v_2 - v_1)}{\Delta x} \right\}^2$$

$$+ \frac{1}{2} C_3 \left\{ \frac{(u_3 - u_2)}{\Delta y} + \frac{(v_3 - v_4)}{\Delta x} \right\}^2$$

$$+ \frac{1}{2} C_4 \left\{ \frac{(u_1 - u_4)}{\Delta y} + \frac{(v_4 - v_3)}{\Delta x} \right\}^2 \quad . \qquad (7)$$

It is desirable to determine an elemental stiffness matrix such that

$$\begin{bmatrix} & & \\ & K_e & \\ & & \end{bmatrix} \begin{bmatrix} u_1 \\ v_1 \\ \cdot \\ \cdot \\ \cdot \\ \cdot \\ u_4 \\ v_4 \end{bmatrix} = \begin{bmatrix} F_{x_1} \\ F_{y_1} \\ \cdot \\ \cdot \\ \cdot \\ F_{x_4} \\ F_{y_4} \end{bmatrix} \qquad (8)$$

This is accomplished by relating the node forces to the partial derivatives of the total strain energy. That is

$$F_{x_i} = \frac{\partial U}{\partial u_i}$$

and (9)

$$F_{y_i} = \frac{\partial U}{\partial v_i} \quad .$$

For example,

$$\frac{\partial U}{\partial u_1} = F_{x_1} = K_{xx}^{12}\left[u_1 - u_1\right] + K_{xy}^{12}\left[\frac{v_1}{2} - \frac{v_4}{2} + \frac{v_2}{2} - \frac{v_3}{2}\right]$$

$$+ \frac{1}{2} C_1 \left[2\left(\frac{v_1 - v_2}{\Delta x\, \Delta y}\right) + \frac{2(u_1 - u_4)}{(\Delta y)^2}\right]$$

$$+ \frac{1}{2} C_4 \left[\frac{2(v_4 - v_3)}{\Delta x\ \Delta y} + \frac{2(u_1 - u_4)}{(\Delta y)^2}\right] \quad . \qquad (10)$$

Expansion of this relation will give the elements in the first row of the matrix $[K_e]$. Subsequent derivatives taken with respect to the other degrees of freedom generate the remaining rows.

The spring constants used in the formulation must be related to the constituent's elastic properties. This is accomplished via the relations

$$K_{xy}^{ij} = Q_{12} \qquad \text{for } i,j = 1,\ldots 4$$

$$K_{xx}^{ij} = Q_{11}\frac{\Delta y}{\Delta x} \qquad \text{for } i,j = 1,\ldots,4$$

$$K_{yy}^{ij} = Q_{22}\frac{\Delta x}{\Delta y} \qquad \text{for all } i,j = 1,\ldots,4$$

$$C_i = \frac{1}{4} Q_{33}\, \Delta x\, \Delta y \quad \text{for all } i = 1,\ldots,4$$

where [Q] is defined as the constitutive stiffness matrix in the usual manner as

$$\begin{bmatrix} \sigma_x \\ \sigma_y \\ \tau_{xy} \end{bmatrix} = \begin{bmatrix} & Q & \end{bmatrix} \begin{bmatrix} \varepsilon_x \\ \varepsilon_y \\ \gamma_{xy} \end{bmatrix} . \tag{11}$$

Specifying these relations is tantamount to assuming that the material in each element is completely homogeneous. The desired heterogenity arises from the fact that the Q_{ij}'s are different for the fiber, matrix, and interface elements.

The Energy-Release Rate

The local rupture criterion used in this work is a generalized version of the ordinary energy-release rate (or crack-driving force) quantity of LEFM. In formulating it, attention must be placed on the complete structure. The discretized form of the equations of equilibrium for a complete structure can be represented by the matrix equation

$$\left[\underset{\sim}{k}\right] \underset{\sim}{u} = \underset{\sim}{F} \quad , \tag{12}$$

where $\underset{\sim}{k}$ is the structural stiffness matrix, $\underset{\sim}{u}$ is the nodal displacement vector and $\underset{\sim}{F}$ the applied nodal load vector. The energy-release rate G can be defined in a global sense by relating it to the change in work done by the applied loading and the strain energy during a virtual crack extension. This is

$$G \equiv \frac{dW}{da} - \frac{dU}{da} \tag{13}$$

where

$$W \equiv \underset{\sim}{u}^T \underset{\sim}{F} \tag{14}$$

is the work done by the applied loading,

$$U \equiv \frac{1}{2} \underset{\sim}{u}^T [\underset{\sim}{k}] \underset{\sim}{u} \tag{15}$$

is the strain energy and a represents the crack length. (In these equations, the superscript T denotes the transpose.)

When Equations (14) and (15) are introduced into Equation (13), it is found that

$$G = \frac{d\underset{\sim}{u}^T}{da} \underset{\sim}{F} - [\underset{\sim}{k}] \underset{\sim}{u} + \underset{\sim}{u}^T \frac{d\underset{\sim}{F}}{da} - \frac{1}{2} \underset{\sim}{u}^T \frac{d}{da} [\underset{\sim}{k}] \underset{\sim}{u} \quad . \tag{16}$$

It can be seen from Equation (12) that the quantity within the braces of Equation (16) is a null vector. Furthermore, if $\underset{\sim}{F}$ is independent of the crack length, then the second term also vanishes. Equation (16) therefore reduces to

$$G = - \frac{1}{2} \underset{\sim}{u}^T \frac{d}{da} [\underset{\sim}{k}] \underset{\sim}{u} \quad . \tag{17}$$

Now, it can be considered that the only contribution to the matrix $\frac{d}{da} [\underset{\sim}{k}]$ is that due to the stiffness matrix K of the element containing the crack tip. If $\underset{\sim}{u}$ denotes the displacement vector of the nodes of the element only, then Equation (17) can be used to obtain an approximation of G that can be written as

$$G = \frac{\underset{\sim}{u}^T [K_b] \underset{\sim}{u} - u^T [K_a] \underset{\sim}{u}}{2\Delta a} \tag{18}$$

where $[K_b]$ ($[K_a]$) is the elemental stiffness matrix before (after) an extension Δa of the crack within the element. Recognizing that

$$U_e = \frac{1}{2} \underset{\sim}{u}^T [K] \underset{\sim}{u} \tag{19}$$

is the elemental strain energy, then an alternative form of Equation (18) is

$$G = \frac{U_{e_b} - U_{e_a}}{\Delta a} \quad . \tag{20}$$

A similar development for the energy-release rate occurs in the recently published papers by Hellen, et al. [6,7].

Program Solution Techniques

To use the analysis that has been developed thus far, the material properties of the constituents and the micromechanical geometry must be specified. (The material properties are also used to determine the homogeneous orthotropic properties of the bulk composite through an effective modulus or volume fraction technique.) The way in which the constituent properties and the geometry are used to generate elemental stiffnesses for assemblage into the LHR will be described next.

There are two classes of nodal points used in the LHR. The first consists of the points on the boundary of the LHR where displacements are prescribed. The nodal points in the interior of the LHR having unknown displacements make up the second class. It is useful to assemble the stiffness matrix in such a way that these two groups are isolated. The partition used here is

$$\begin{bmatrix} [k_{22}] & [k_{23}] \\ [k_{32}] & [k_{33}] \end{bmatrix} \begin{Bmatrix} \{u_2\} \\ \{u_3\} \end{Bmatrix} = \begin{Bmatrix} \{F_2\} \\ \{F_3\} \end{Bmatrix} \quad . \tag{21}$$

In Equation (21), the subscripts do not refer to nodes, but to the nodal point classification just described. That is (u_2) represents the prescribed displacement vector of the peripheral points while (u_3) is the vector of the unknown displacements for which a solution is desired. Note that the number 1 was not used as a subscript because it is more convenient to reserve it for specified zero displacements.

By performing the matrix multiplication indicated in Equation (21), the following two equations are obtained:

$$[k_{22}] \{u_2\} + [k_{23}] \{u_3\} = \{F_2\} \tag{22}$$

$$[k_{32}] \{u_2\} + [k_{33}] \{u_3\} = \{F_3\} = \{0\} \quad . \tag{23}$$

Most often, it is either impossible or inefficient to store large matrices such as $[k_{33}]$ in the computer's central processor core area. For this reason $[k_{33}]$ is stored externally. The external storage can be minimized by utilizing the fact that the $[k_{33}]$ matrix is always symmetric and banded; the latter term indicating the tendency for nonzero values to cluster around the diagonal of the matrix. By taking advantage of matrix partitioning (i.e., the grouping of prescribed and unprescribed degrees of freedom), symmetry, and the banded nature of the stiffness matrix, storage of only a small portion of the original total stiffness matrix is required. However, this reduced storage requirement can still be very large in some problems.

Solution of Equation (23) is accomplished through the use of Gaussian elimination with back substitution. Small parts of stored $[k_{33}]$ matrix are brought into core as required in this operation. Assemblage of the required parts of the stiffness matrix is done by the direct stiffness method.* Components that would ordinarily fall within the $[k_{22}]$ and $[k_{23}]$ submatrices are discarded. Stiffness components that fall within the $[k_{32}]$ submatrix are used in a nonzero $\{F_3\}$ vector. Finally, those values of $[k_{33}]$ falling on or above its diagonal are stored externally.

Once the boundary conditions have been prescribed, an out-of-core type solution of the partitioned LHR stiffness matrix with boundary conditions for a unit load is performed. The resulting displacement vector is then used to calculate the potential fracture energies associated with each of the four fracture codes. Ratios of the prescribed critical energy levels to these calculated energies are next computed. The applied load is then adjusted such that the highest ratio becomes exactly equal to unity. This critical region (if one exists) is allowed to break in one of the four ways (codes) described above. Appropriate modifications are then made to the LHR stiffness matrix.

* A detailed description of the direct stiffness assemblage technique used in this work is given by Desai and Abel [8].

Because the system is completely linear elastic, a solution for another load level can then be performed in exactly the same manner. In this way, the properties of a crack tip damage zone as a function of an increasing applied load can be generated.

As each local rupture occurs, the prescribed boundary conditions must be adjusted. If the crack has propagated in a self-similar fashion, this is readily done by shifting the origin (cf, Figure 2). If not, this may present some very real difficulties for then the continuum solution no longer exactly applies and some approximations must be used for setting the boundary conditions. The larger the LHR, the less likely this will be necessary. Of course, large LHR's require large solution times even though storage is generally not a problem because of the out-of-core solution. It is likely that the boundary condition problem can be handled by introducing a flexible boundary-condition scheme (see Recommended Future Research section), or, possibly, by allowing the fractured LHR to interact in a hybrid continuum model for future boundary updating.

Verification of Computational Model

Before performing extensive calculations on composite materials, it is appropriate to verify the computational model by checking it against known solutions. By letting the model represent a linear elastic homogeneous material, two checks can be made. These are on the displacements in the LHR and on the calculated energy-release rate.

Consider the element configuration shown in Figure 1. A check on the calculated displacements can be made by imposing the continuum derived boundary conditions on a LHR region where the LHR is used to simulate a completely homogeneous region. Displacements at the node points were calculated and used to calculate average stresses within the elements. The computed values of stress and displacement were then compared with values calculated by the continuum solution for the interior of the region. Agreement between the two solutions was found to be quite good. The check thus provided one necessary verification of both the LHR element itself and of the finite element assemblage and solution procedure as well.

As described in the above, all of the energy released within the element at the crack tip, if an incremental amount of crack extension were to occur, should equal the strain energy-release rate, G. To check this, cal-

culations were made using the exact near crack tip displacement field for an elastic isotropic material. The energy-release rate obtained from this calculation is denoted by G^* to distinguish it from the exact theoretical value G. The necessity for introducing this distinction is as follows.

The quantity G can be formally defined in terms of a virtual crack extension as the total change in energy of the body per unit area of crack extension; cf, Equation (13). The quantity G^*, on the other hand, reflects only the change in energy of the element near the crack tip. Consequently, G^* does not include the change in energy of the remainder of the body as the crack extends. In order to account for the contribution arising from the change in energy of the remainder of the structure, a term denoted by δG^* was formulated. The sum $G^* + \delta G^*$ is then taken as the appropriate approximation to G in this work.

A numerical experiment was performed to calculate G^* and δG^* as a function of the aspect ratio $\Delta y/\Delta x$ of the LHR elements. The results are shown in Table II. It is quite evident that the sum $G^* + \delta G^*$ provides an accurate approximation to G for the elongated aspect ratios that are convenient to use in the calculations on fiber composite materials.

There are two further points of interest about the results shown in Table I. First, while it may be surprising that δG^* and G^* are functions only of the ratio of Δy to Δx, this is a direct consequence of the use of rigid boundary conditions which put the near tip displacements into the energy relationship used to calculate G. The resulting expression contains only the aspect ratio, $\Delta y/\Delta x$. Second, while it might be expected that δG^* should converge to zero as the grid spacing is collapsed (i.e., as both $\Delta y \to 0$ and $\Delta x \to 0$), it can be seen that this was not the case. Instead, convergence is obtained only as the ratio of Δy to Δx becomes large. Then, δG^* approaches a value equal to 11 percent of G while G^* converges to value equal to 86 percent of G.

A number of different computations for heterogeneous materials have also been made. These runs have been made with a model similar to the one shown in Figure 3. Preliminary results indicate that most of the initially envisioned modes of failure are exhibited by the model. A discussion of these results is given in the next section of this report.

TABLE I. AN EXAMPLE CALCULATION OF THE STRAIN ENERGY RELEASE RATE AS A FUNCTION OF THE GRID SIZE RATIO FOR A HOMOGENEOUS LINEAR ELASTIC MATERIAL

$\frac{\Delta y}{\Delta x}$	$\frac{G^*}{G}$	$\frac{\delta G^*}{G}$	$\frac{(G^* + \delta G^*)}{G}$
1	0.71	0.75	1.46
2	0.72	0.42	1.14
4	0.77	0.25	1.02
8	0.81	0.18	0.99
16	0.83	0.15	0.98
32	0.84	0.13	0.97
64	0.85	0.12	0.97
128	0.86	0.11	0.97
256	0.86	0.11	0.97

EXAMPLE COMPUTATIONAL RESULTS FOR FRACTURE OF FIBER-REINFORCED COMPOSITES

A number of computations have been performed using the analysis technique described in the preceding section of this report. As discussed in this section, the results demonstrate the ability of the model to exhibit most of the actual failure mechanisms in fiber-reinforced composite materials. These include fiber-matrix debonding, fiber bridging, matrix bridging, and matrix crazing. The only important micromechanical mechanism that the model currently does not explicitly represent is fiber pull-out.*

Calculations With Arbitrarily Varied Rupture Properties

The following describes a series of example calculations in which the various fracture mechanisms are made to manifest themselves. The results shown here were obtained by varying each of the constituent's rupture properties and, in some instances, the constituent elastic properties, over a wide range of values. Hence, the actual values selected to perform these example computations are not totally realistic. The intent here is to provide a qualitative verification that the model is capable of achieving its primary function rather than to make realistic predictions.

Unless otherwise stated, the elastic constants used in the calculations are those given in Table II.

TABLE III. ELASTIC PROPERTIES USED IN THE SIMULATION OF A GRAPHITE EPOXY COMPOSITE

Constituent	E Elastic Modulus (ksi)	ν Poisson's Ratio
Fiber	28,000	0.3
Matrix	495	0.3
Interface	495	0.3

* As discussed in the Recommended Future Research section of this report, steps to incorporate both fiber pull-out and interply delamination can be performed in a straightforward manner in subsequent work.

These properties were intended to be nominally equivalent to those of a graphite epoxy composite with a volume fraction of fiber equal to 70 percent. Consistent with these values are the following properties of the bulk composites:

$$E_1 = 18{,}000 \text{ ksi}, \quad \nu_{12} = 0.25$$

$$E_2 = 690 \text{ ksi}, \quad G = 3{,}000{,}000.$$

Note that the constituents were assumed to be isotropic. However, the model does not require this.

The first computation to be discussed is shown in Figure 6. This result illustrates the fiber-matrix debonding mechanism, a mechanism that occurs in a large number of cases. Typically, a crack will advance through the matrix and then vertically separate or axially split the interface. In this example, the interfacial elements were made relatively weak while the fiber and matrix material were given relatively average strengths. The loading in this example was purely Mode I.* It was found that axial splitting is even more prevalent when Mode II loads are applied.

Matrix crazing typically occurs when a crack advancing through the matrix reaches a very strong stiff fiber. Figures 7 and 8 show typical examples. If the fiber does not break, a number of local events occur in the matrix that seem to approximate matrix crazing. Typically, the crazing does not occur on the uncracked side of the fiber. The reason is that the displacements on the cracked side of the fiber are "locked in" by the adjacent highly stretched fiber. Consequently, crazing usually occurs when strong very stiff fiber properties are inserted into the model together with average strength and stiffness properties for the matrix and interface.

Matrix bridging is shown in Figure 9. This phenomenon typically occurs when the fibers are considered to be stiff, but weak. In these instances the matrix and interface are capable of withstanding higher elongation than the fiber. So, they will remain intact while the fiber cracks. In the example shown in Figure 9, some additional interfacial response can also be noticed.

---

* Unless otherwise stated, in the calculations described in this section of the report, the applied loading was a tensile normal stress in the direction parallel to the fibers.

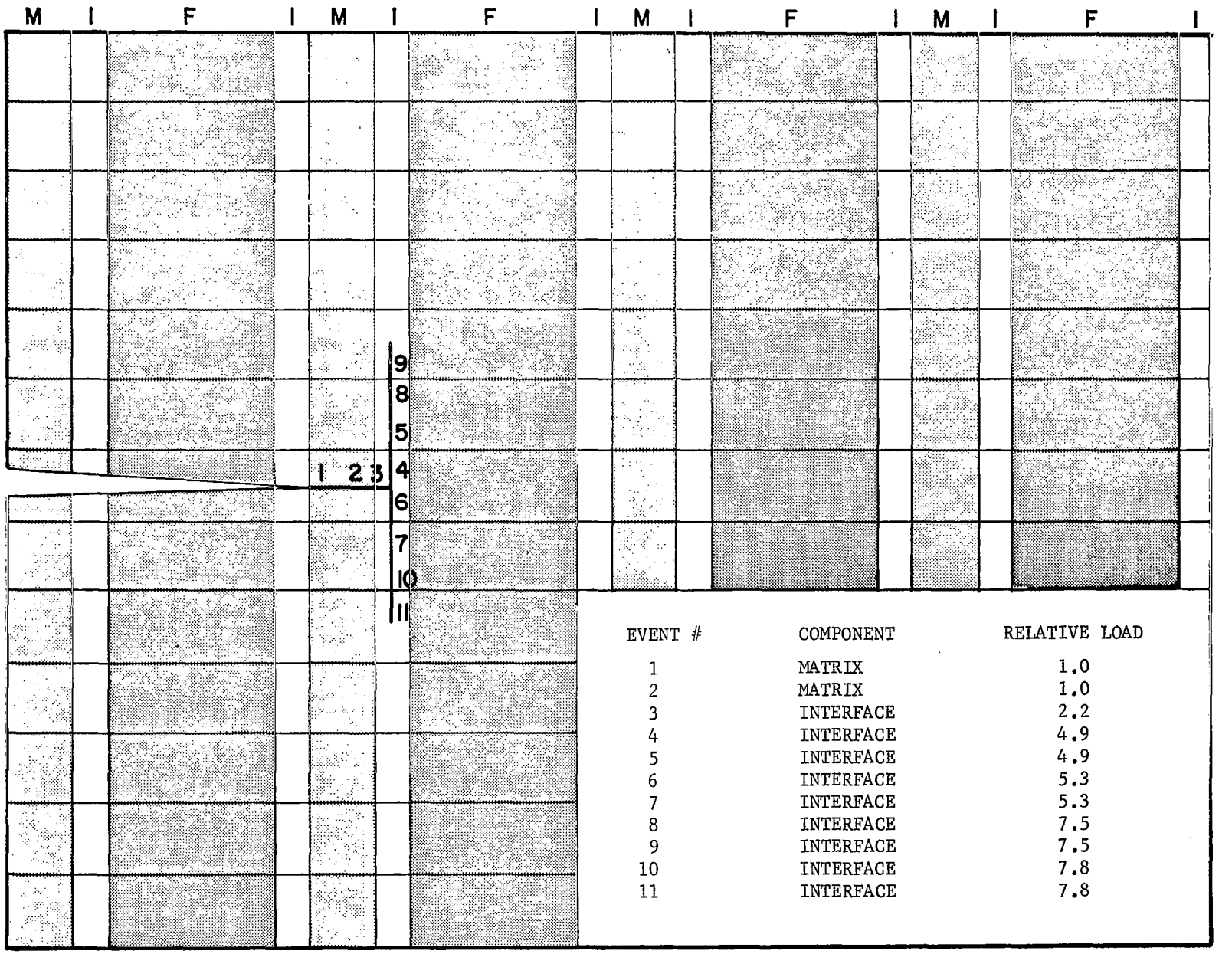

EVENT #	COMPONENT	RELATIVE LOAD
1	MATRIX	1.0
2	MATRIX	1.0
3	INTERFACE	2.2
4	INTERFACE	4.9
5	INTERFACE	4.9
6	INTERFACE	5.3
7	INTERFACE	5.3
8	INTERFACE	7.5
9	INTERFACE	7.5
10	INTERFACE	7.8
11	INTERFACE	7.8

FIGURE 6. EXAMPLE CALCULATION WITH WEAK INTERFACE SHOWING MATRIX-FIBER DEBONDING

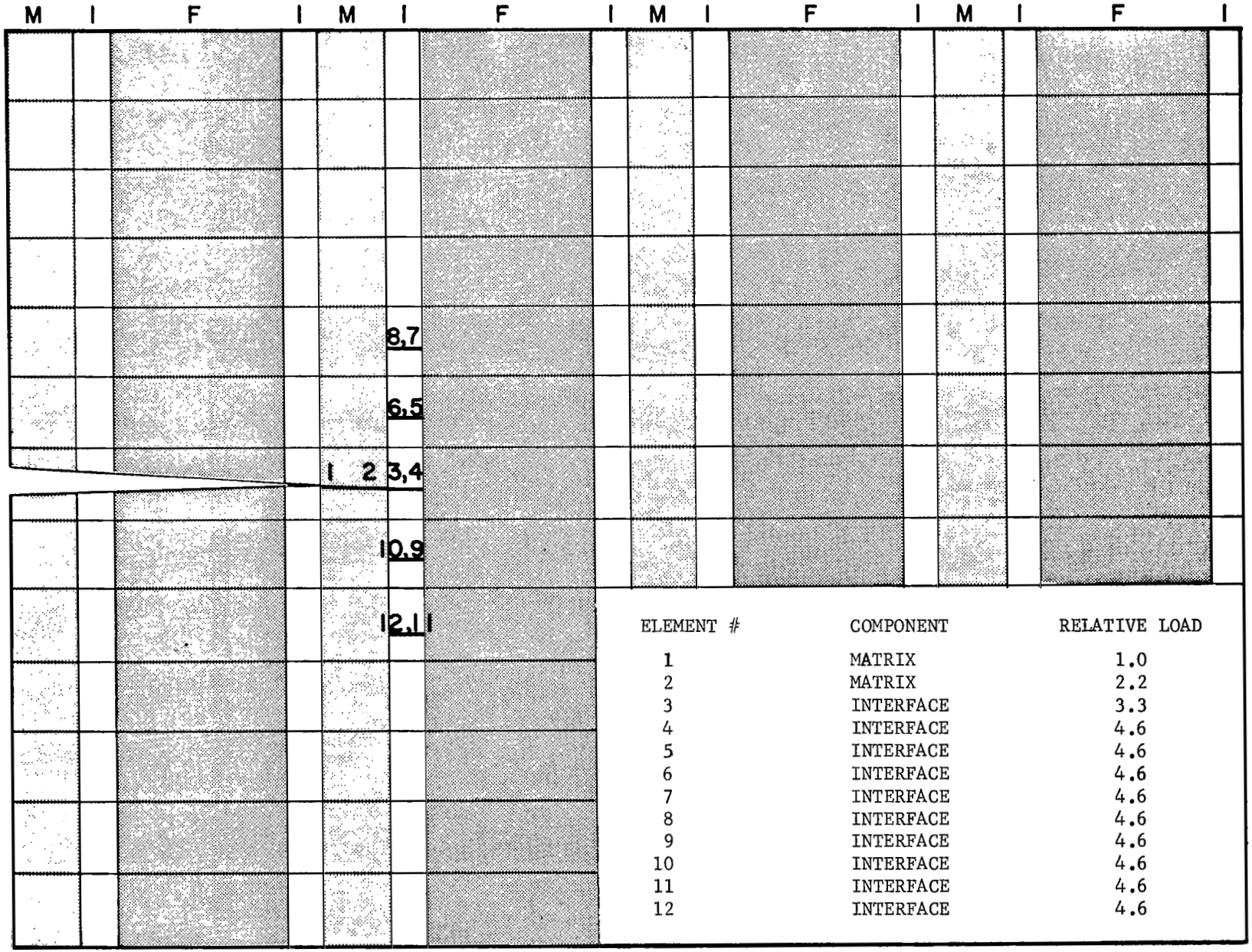

ELEMENT #	COMPONENT	RELATIVE LOAD
1	MATRIX	1.0
2	MATRIX	2.2
3	INTERFACE	3.3
4	INTERFACE	4.6
5	INTERFACE	4.6
6	INTERFACE	4.6
7	INTERFACE	4.6
8	INTERFACE	4.6
9	INTERFACE	4.6
10	INTERFACE	4.6
11	INTERFACE	4.6
12	INTERFACE	4.6

FIGURE 7. EXAMPLE CALCULATION WITH STRONG STIFF FIBERS AND WEAK INTERFACE SHOWING MATRIX CRAZING

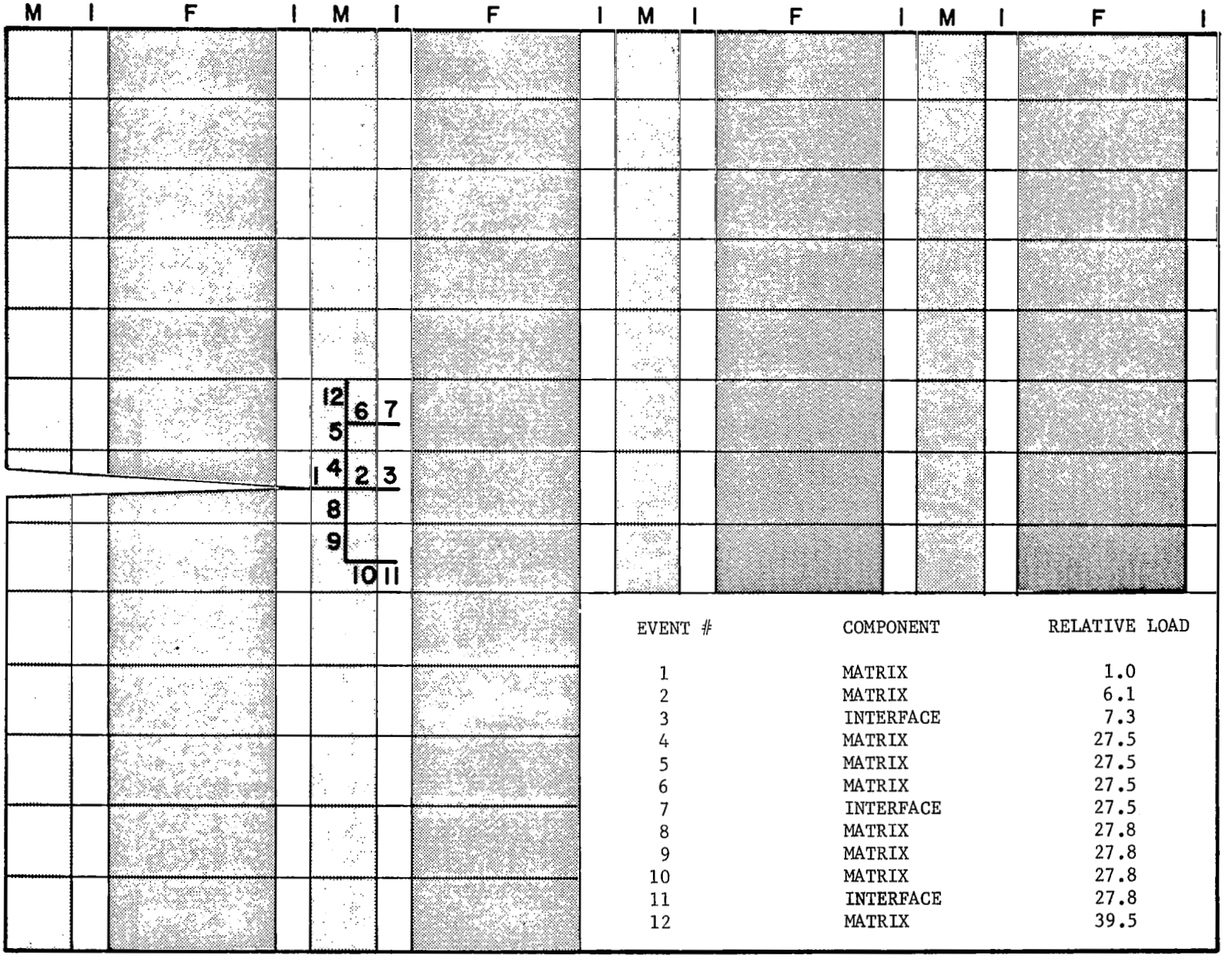

EVENT #	COMPONENT	RELATIVE LOAD
1	MATRIX	1.0
2	MATRIX	6.1
3	INTERFACE	7.3
4	MATRIX	27.5
5	MATRIX	27.5
6	MATRIX	27.5
7	INTERFACE	27.5
8	MATRIX	27.8
9	MATRIX	27.8
10	MATRIX	27.8
11	INTERFACE	27.8
12	MATRIX	39.5

FIGURE 8. EXAMPLE CALCULATION WITH STRONG STIFF FIBERS SHOWING MATRIX CRAZING

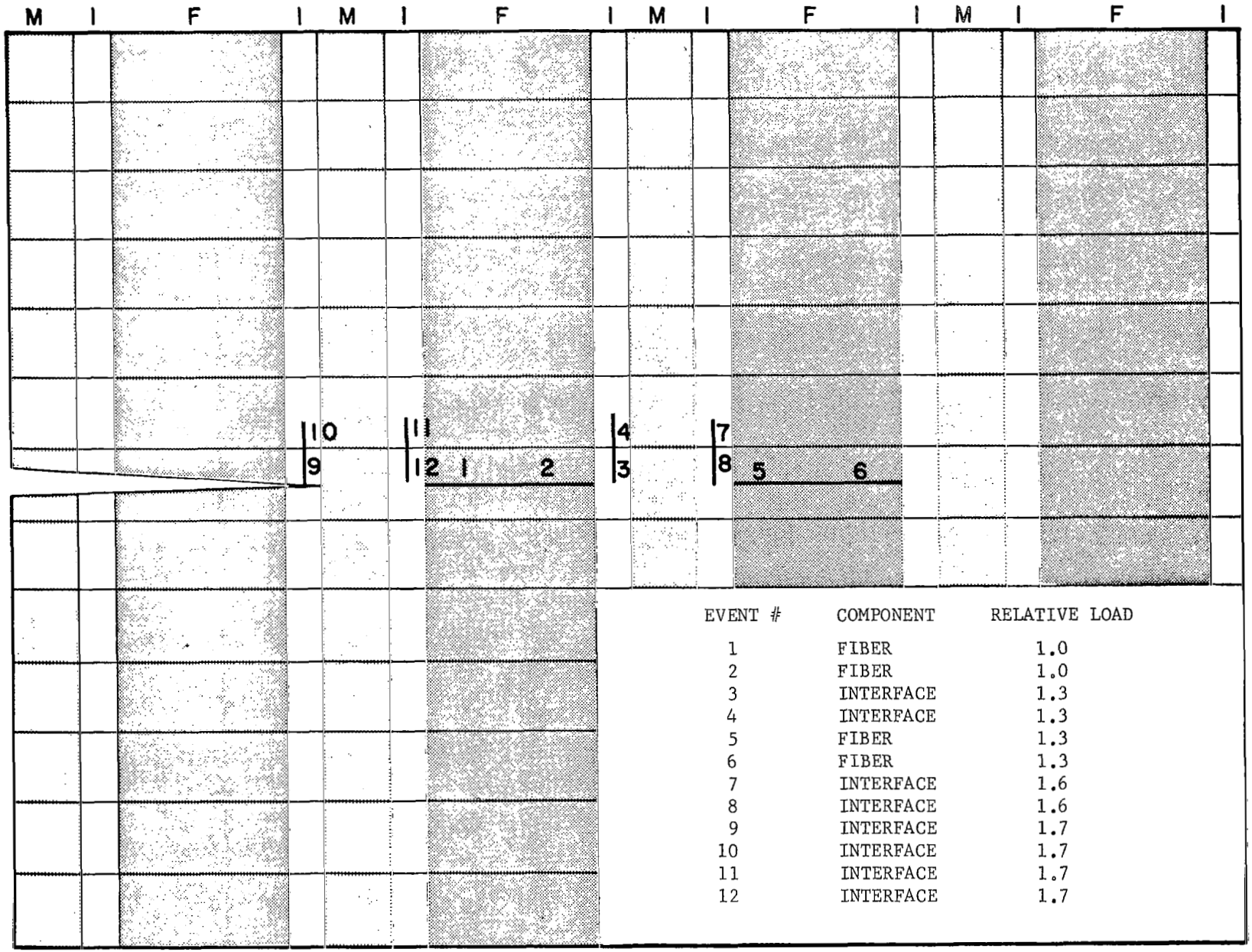

EVENT #	COMPONENT	RELATIVE LOAD
1	FIBER	1.0
2	FIBER	1.0
3	INTERFACE	1.3
4	INTERFACE	1.3
5	FIBER	1.3
6	FIBER	1.3
7	INTERFACE	1.6
8	INTERFACE	1.6
9	INTERFACE	1.7
10	INTERFACE	1.7
11	INTERFACE	1.7
12	INTERFACE	1.7

FIGURE 9. EXAMPLE CALCULATION WITH STIFF WEAK FIBERS SHOWING MATRIX BRIDGING

Fiber bridging is more prevalent when the fiber modulus does not greatly exceed the matrix modulus. (In graphite epoxy, the modulus ratio is on the order of 50 and fiber bridging does not then seem to occur.) Figure 10 demonstrates this behavior. Fiber bridging can also be related to the microstructural geometry. That is, in computations performed with relatively thin fibers, this mechanism becomes more dominate.

It should be emphasized that the examples given in the above deliberately used exactly the same LHR configuration and applied loading. The program has the flexibility to consider different loading conditions and LHR geometries. However, this option was not exercised here because of the complications that would be added to the interpretation of the results. That is, it would be difficult to separate the effects due to the LHR geometry and loading from those due to variations in the rupture strength and modulus. Such calculations will be deferred until further refinements have been incorporated into the model. Again, the purpose of the computations given in Figures 6-10 is to give a qualitative demonstration that the model is capable of coping with the micromechanical failure processes involved in the fracture of composite materials, not to produce precise quantitative results.

Finally, note that the relative load levels at which each individual fracture event occurs is recorded. (These levels are relative to the load level at which the initial rupture event occurs.) It can be seen that the load level must ordinarily be increased to obtain additional rupture events, or, in other words, in order to enlarge and propagate the crack-tip damage zone. This can be contrasted with the behavior of completely homogeneous, perfectly brittle materials represented by LEFM where crack extension, once initiated, would continue in a catastrophic manner under a constant load level. The initial stages of the fracture event in fiber composite materials therefore can obviously be characterized in terms of a stable growth process. This suggests that a modification of the crack growth resistance curve (R curve) approach developed for the fracture of ductile materials could be useful for studying fractures in fiber composite materials. Such an approach, it might be mentioned, has already been suggested in the literature; for example, by Gaggar and Broutman [9]. However, these approaches are usually semiempirical in nature, relying heavily on LEFM concepts. The present approach, in contrast, should be able to make a direct prediction of the crack growth resistance parameter purely from fundamental-level considerations.

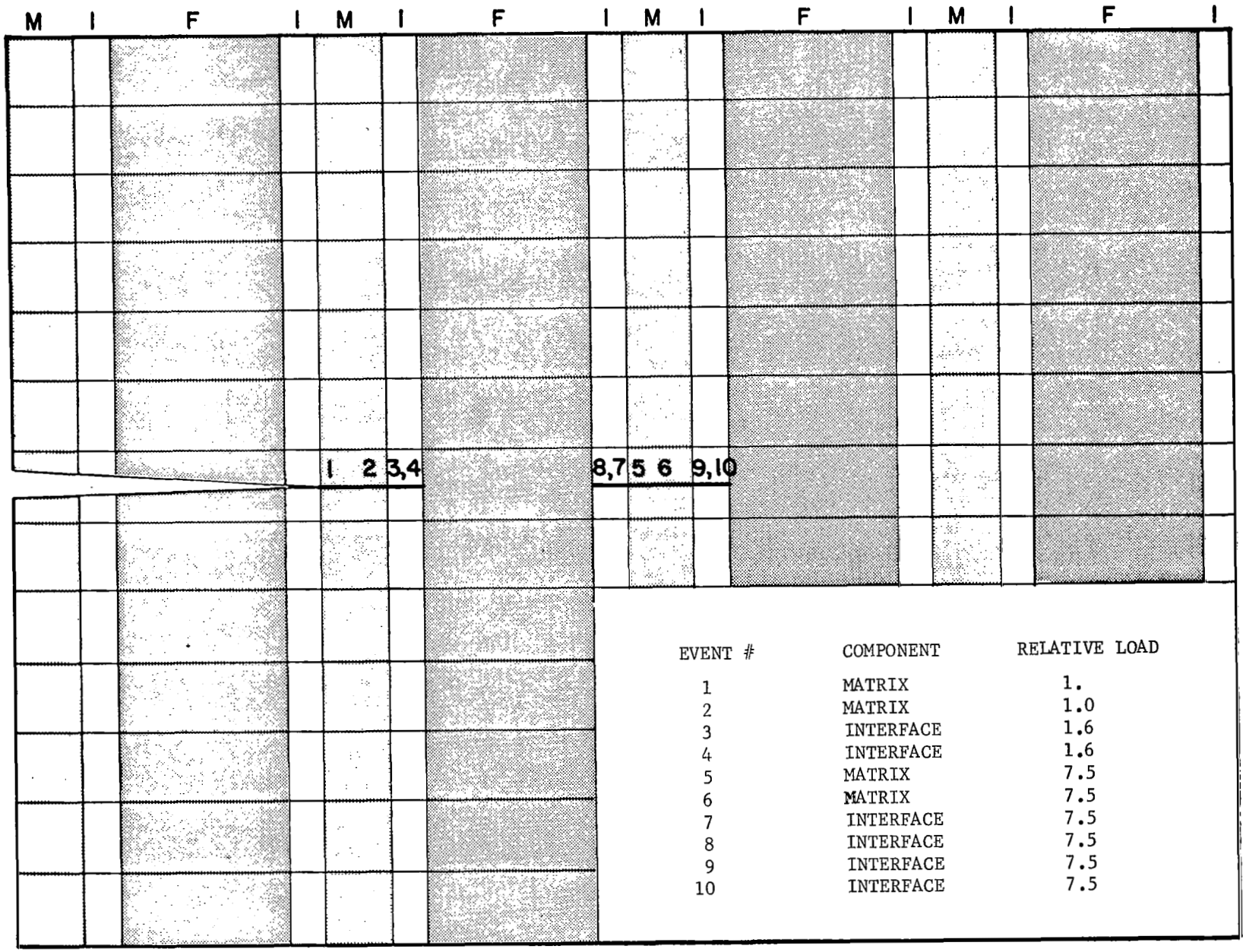

FIGURE 10. EXAMPLE CALCULATION WITH STIFF MATRIX SHOWING FIBER BRIDGING

Comparison of Calculated Results with VPISU Experimental Data

The computations described in the preceding section demonstrate that the model developed in this report displays the various micromechanical failure mechanisms actually exhibited by fiber reinforced composites. A more quantitative verification is also possible. This can be done by comparing the predictions of the model with the experimental results obtained in the concurrent NASA-Ames sponsored research at Virginia Polytechnic Institute and State University (VPISU) by Brinson and Yeow [10]. They have measured the strengths of both unidirectional and angle ply graphite/epoxy composites using unnotched, single edge notched, and double edge notched specimens with the crack introduced at various angles to the fiber direction. In this section, the model will be used to estimate the strengths of some of the Brinson-Yeow unidirectional notched tests using input values inferred from their unnotched tests.

A precise prediction of failure loads is not to be expected at the present stage of this research for several reasons. First, because of the stable damage growth that precedes fracture in composites, computations performed using rigid boundary conditions (which artifically constrain the damage growth process) will not be realistic. The predictions of the initial local failure event--the threshold of stable damage growth--should be reasonably well predicted, however. This load level will therefore be taken as the prediction of the model to be compared with the experimental measurements. It should be recognized that, because of the neglect of the stable growth regime, these should underestimate the actual failure loads.

A second reason for the lack of precision inherent in the present predictive capability is that the constituent properties needed in the model have not been properly determined as yet. As in the preceding section, linear elastic-perfectly brittle behavior can be assumed with handbook values being taken for the elastic properties. Rupture properties are not as readily available, however. To circumvent this difficulty, the experimental results on unnotched specimens obtained by Brinson and Yeow can be used. Their data on the strengths of unnotched coupons pulled to failure with the load in the fiber direction ($\theta = 0°$) and normal to the fiber direction ($\theta = 90°$) are given in Table III. Relying on their observation that matrix failure occurred in

TABLE III. CRITICAL VALUES FOR MATRIX FAILURE
IN GRAPHITE EPOXY COMPOSITES

Angle Between Load and Fiber Directions	Experimental Values[a]			Critical Strain Energy Density (in. lb/in.^{3})
	Elastic Modulus (ksi)	Fracture Stress (ksi)	Fracture Strain (%)	
0°	18,200	154.7	0.82	576
90°	1,700	6.1	0.44	13.6

(a) Data of Brinson and Yeow [10] on unidirectional unnotched specimens for a loading rate of 2 x 10^{-3} inches/min.

virtually all cases, the critical strain energy density quantity can be calculated (i.e., $\frac{1}{2}E\varepsilon^2$) for use in the model. These figures are given in the last column in Table III.

As discussed on page 11 of this report, the applied loads acting on the body are communicated to the crack tip elements via the anisotropic elastic stress intensity factors. For test specimens, such as the single and double edge notched configurations used by Brinson and Yeow, there is a term in the stress intensity factor that contains the effects of the finite geometry. This term is not the same for anisotropic and isotropic bodies. However, in view of the approximate nature of the present calculations, the refinement added through the use of the rather complicated anisotropic expression was not believed to be warranted. Hence, the isotropic expressions were used. For Mode I loading, these have the form.

$$K_I = \sigma a^{\frac{1}{2}} Y \tag{24}$$

where σ is the applied stress normal to the crack plane, a is the crack length and Y is a dimensionless function of the specimen geometry. For the double edge notched configuration

$$Y = 1.99 + 0.76\left(\frac{a}{W}\right) - 8.48\left(\frac{a}{W}\right)^2 + 27.36\left(\frac{a}{W}\right)^2 , \tag{25}$$

while for the single edge notched configuration

$$Y = 1.99 - 0.41\left(\frac{a}{W}\right) + 18.7\left(\frac{a}{W}\right)^2 - 38.48\left(\frac{a}{W}\right)^3 + 53.85\left(\frac{a}{W}\right)^4 , \tag{26}$$

where W is the plate width.

For a given crack length and load-fiber orientation in either the single or double edge notched configuration, the load corresponding to the threshold of damage is determined by a single calculation. This is due to the linear elastic material behavior assumed in the current model. That is, a computation can be performed for an estimated value of K_I. The solution can then be scanned to determine the highest strain energy density in any matrix element. By "scaling up" the solution to force this value to match

the critical value given in Table IV, the value of K_I corresponding to the threshold of damage is determined. The final step is to use Equation (24) to calculate the applied stress for direct comparison with the experimental results.

Comparisons of the calculated results as a function of crack length with the Brinson-Yeow results on unidirectional composites are shown in Figures 11 and 12 for the single and double edge notch configurations, respectively. Note that a semilog format is used (so that both the 0° and the 90° fiber-load angle results can be shown on the same plot) and this may make the agreement appear to be better than it really is. Nevertheless, in view of the remarks made in the preceding section, the prediction is reasonably accurate and, as expected, generally provides a lower bound to the experimental data. Note also that the unnotched result ($\frac{a}{W} = 0$) is included on the theoretical curve to emphasize that this point was used to construct the curve.

Finally, comparisons with experimental data can also be made for the case of cracks introduced at an angle to the fiber direction. An example computation is shown in Figure 13. The threshold-of-damage load level calculations are made as above except that both the Mode I and Mode II stress intensity factors now are involved in the computation. These have been taken as

$$K_I = \sigma a^{\frac{1}{2}} Y \sin^2 \phi$$

and

$$K_{II} = \sigma a^{\frac{1}{2}} Y \cos \phi \sin \phi \quad , \tag{27}$$

where ϕ is the angle between the crack plane and the fiber direction. A comparison between the predicted results and the Brinson-Yeow experimental results as a function of ϕ for a 0° load-fiber angle is shown in Figure 14. Again, it can be seen that the model provides a reasonable lower bound to the experimental results.

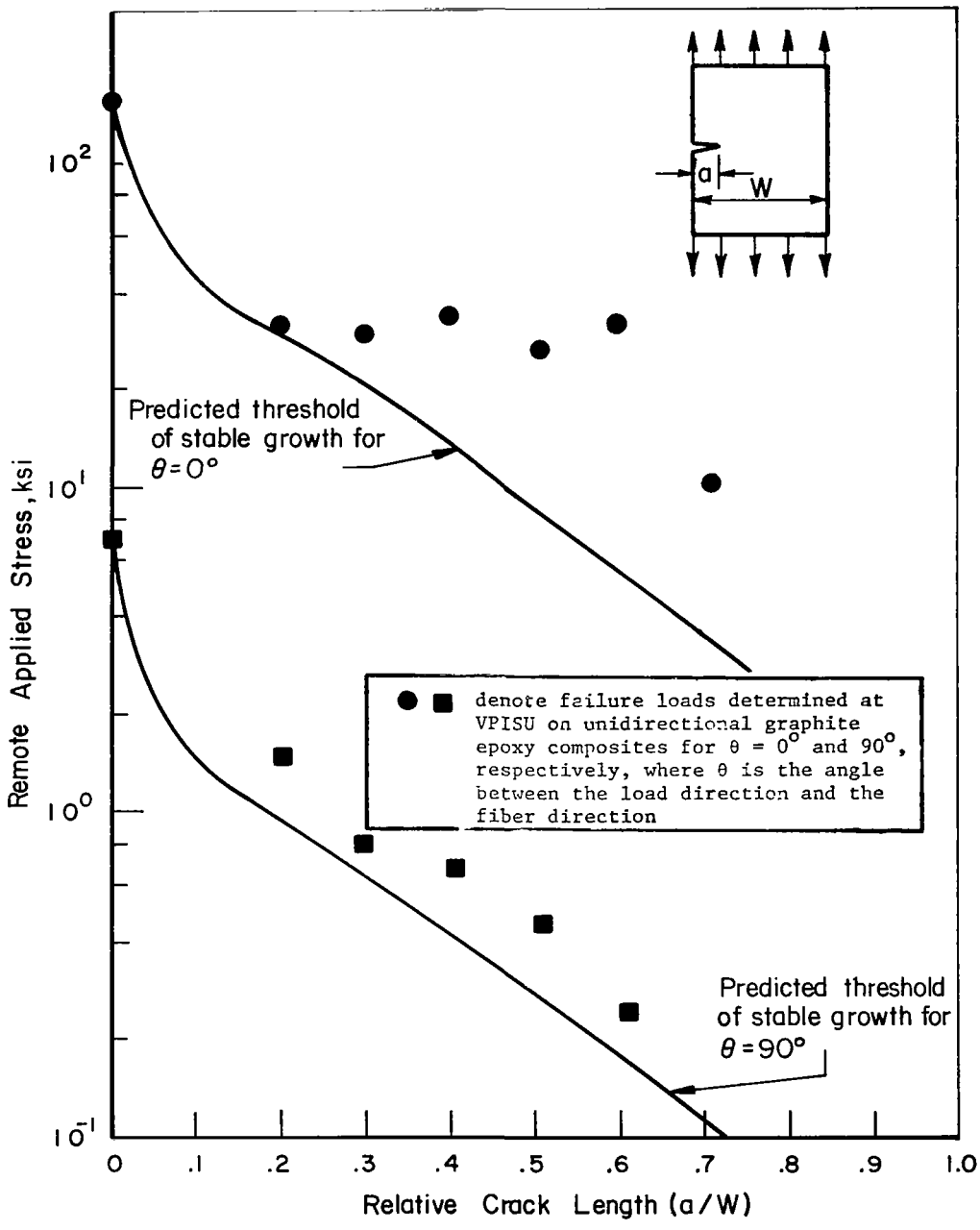

FIGURE 11. COMPARISON OF PREDICTED STABLE GROWTH THRESHOLD WITH EXPERIMENTAL FAILURE LOADS FOR SINGLE EDGE NOTCH SPECIMENS

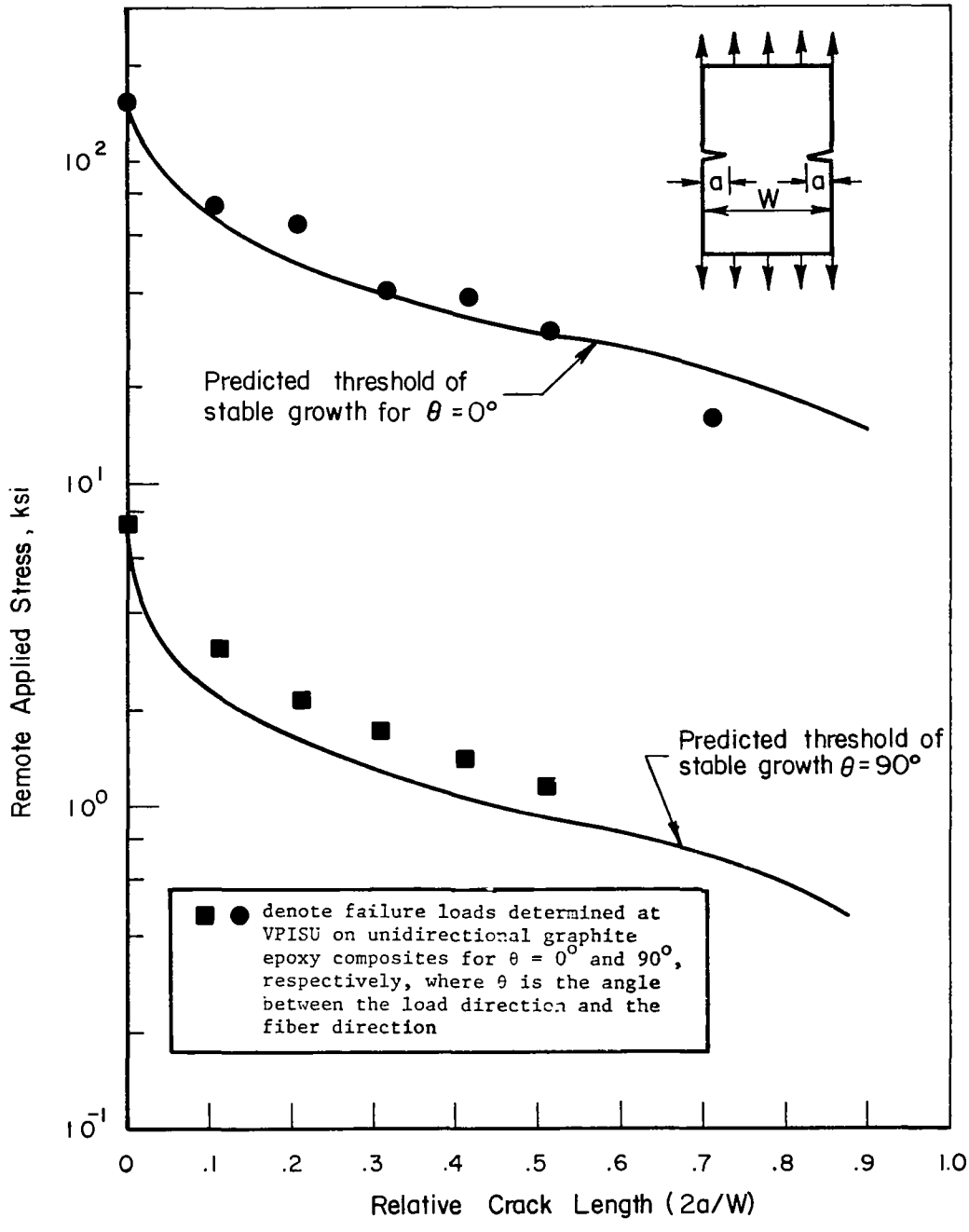

FIGURE 12. COMPARISON OF PREDICTED STABLE GROWTH THRESHOLD WITH EXPERIMENTAL FAILURE LOADS FOR DOUBLE EDGE NOTCH SPECIMENS

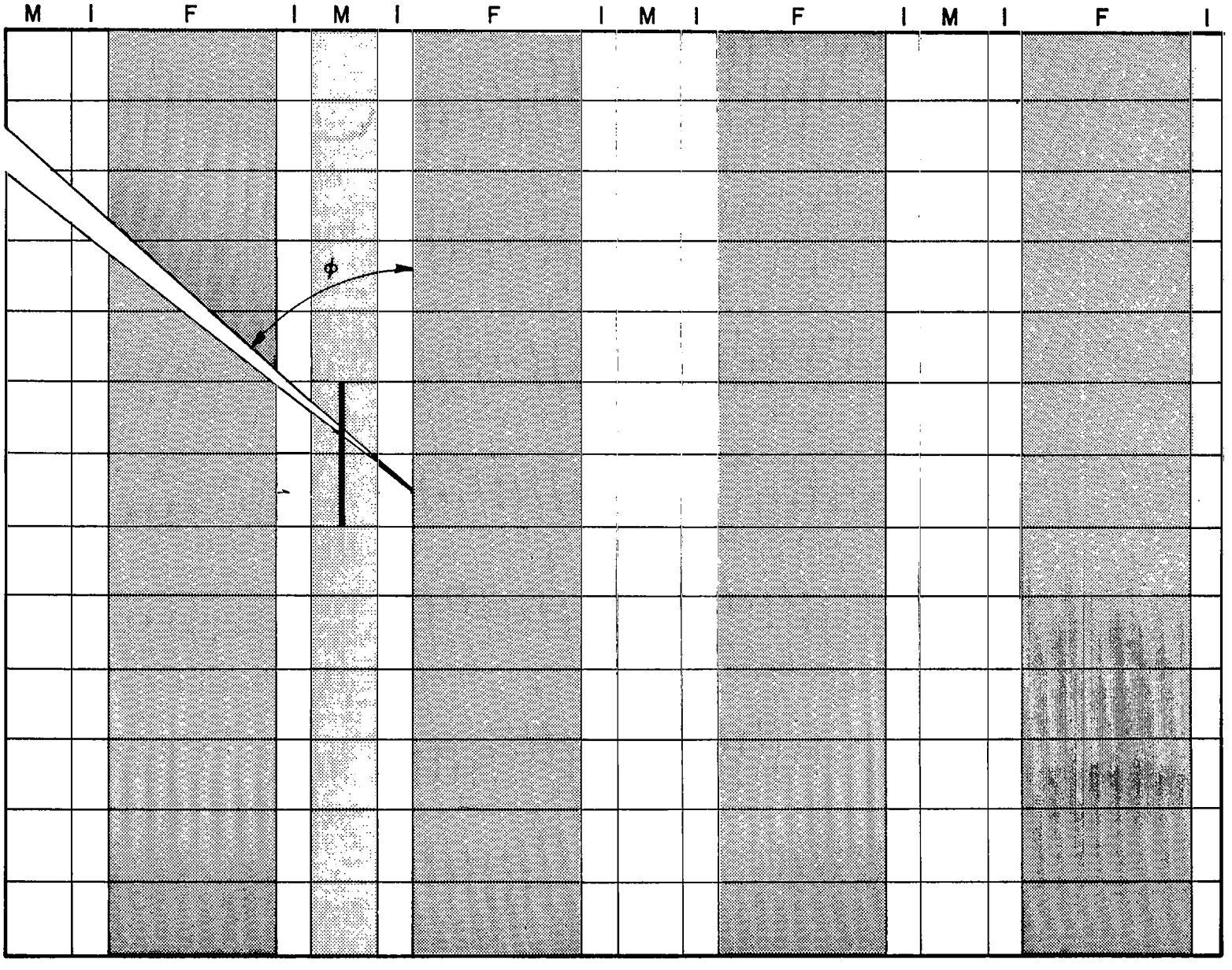

FIGURE 13. EXAMPLE CALCULATION FOR A FIBER COMPOSITE WITH AN ANGLE CRACK

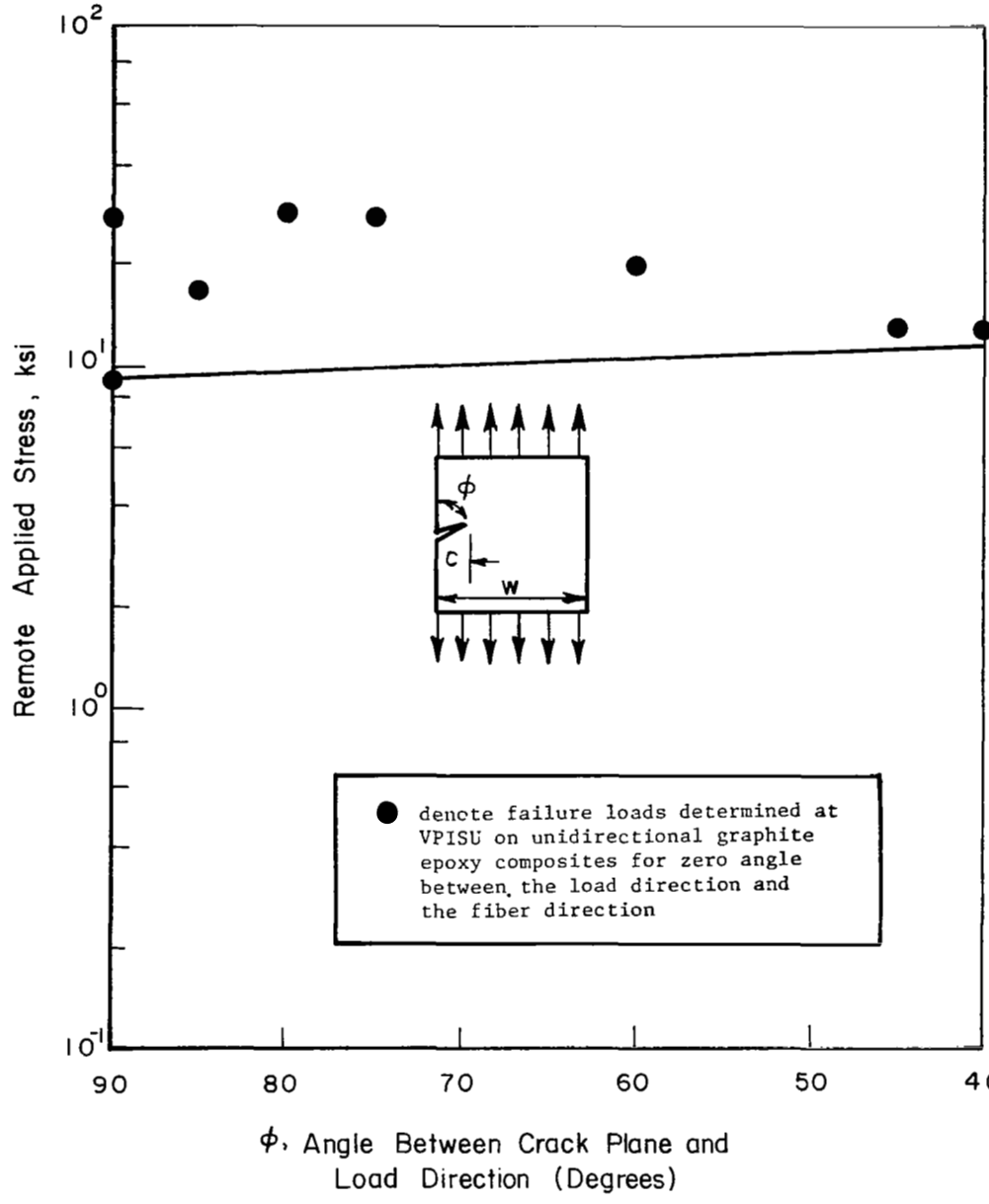

FIGURE 14. COMPARISON OF PREDICTED STABLE GROWTH THRESHOLD WITH EXPERIMENTAL FAILURE LOADS FOR SINGLE EDGE NOTCH SPECIMENS WITH ANGLE CRACKS

RECOMMENDED FURTHER RESEARCH

Being two dimensional, the model described in this report is so far limited in application to unidirectional laminates and can only reflect the local damage modes that occur in plane deformation. In subsequent work, it would be desirable to extend the model from two dimensions to three dimensions to treat angle ply laminates. In addition to treating the effect of different layups, new modes of damage (e.g., interply delamination, fiber pull-out) should also be included.

A straighforward extension of the model could be made by devising a three-dimensional LHR. But, the number of storage locations required for the three-dimensional grid would likely exceed the fast access storage of most computers. To circumvent this situation, the present two-dimensional model could be extended to angle ply laminates by considering laminates with an LHR only in a single ply. Figure 15 shows this concept. In the simplest case, the LHR can be confined to the most critical ply as the load level is increased. In general, there can be an LHR in each ply with attention shifted from one ply to another in turn. In either case, it would be necessary to assume that the interply interactions are not affected by the precise details of the local damage occurring in each ply.

In Figure 15a, a laminate containing a flaw is shown with generalized loading conditions. In this the first level of modeling, all of the plys are considered as homogeneous orthotropic layers. Displacements can be calculated in this model for any load level and applied to the boundaries of the local homogeneous region in each ply. Then, just as in the two-dimensional model, the LHR shown in Figure 15b can be monitored to determine the local rupture events and the extent of the damage zone at that load level. When significant crack growth has occurred in one or more plys, the first level model must, of course, be made to reflect this. But, the basic approach would not be changed thereby.

Two distinct techniques must be developed in order to obtain an accurate set of boundary displacements for each LHR when extensive damage occurs in that or in neighboring plys. The first is to incorporate the effect of the stiffness change in the LHR into the first level model of the laminate. The loading conditions would then be obtained from this modified first level model (i.e., one with locally reduced stiffnesses) to give the new boundary

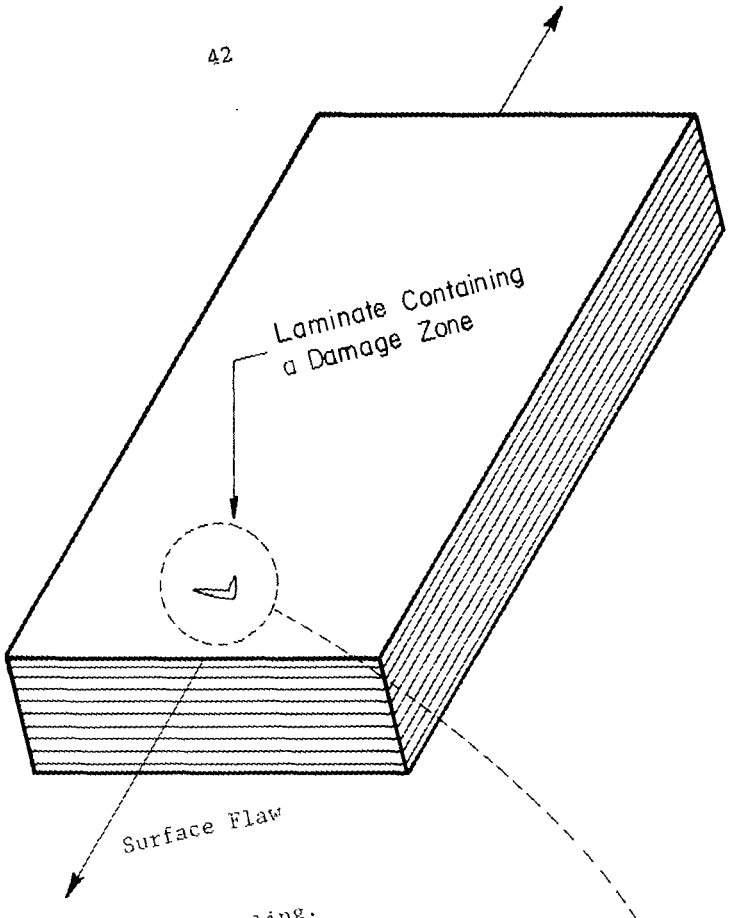

(a) First level of modeling.

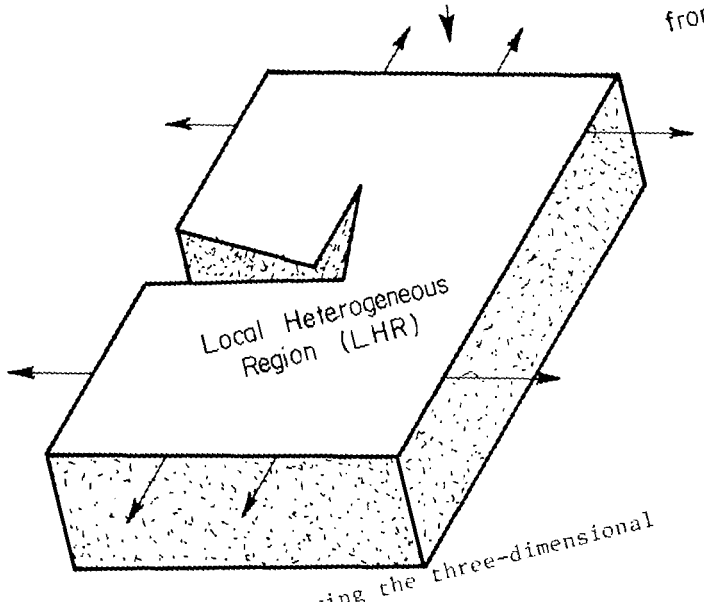

ing showing the three-dimensional

PLATE

conditions for the LHR. In the second technique, the influence of the stiffness of the laminate away from the crack tip will be directly transferred to the LHR through what can be called a "flexible boundary condition" technique. This approach can be likened to placing a series of springs on the LHR boundary with stiffnesses taken from the first level model. The actual technique is more sophisticated than this, however, as follows.

In the work described so far, the peripheral elements in the LHR have been positioned according to the displacement field given by a completely linear elastic continuum solution for the given crack tip location and applied loads. This is not strictly correct even when the displacements are periodically updated as the crack extends in the LHR. Even in the absence of local damage, the highly nonlinear inhomogeneous nature of the crack-tip region in a composite will cause significant departures from the continuum displacements. A scheme for estimating these displacements based on a determination of the equilibrium state between the LHR and the continuum can be obtained by adapting the technique reported in Reference 3. Such a scheme has been referred to as the "flexible boundary condition" approach. The approach used so far can be called the "rigid boundary condition" approach because, even with periodic updating to reflect the progress of the crack through the LHR, the LHR does not directly affect the continuum region surrounding it. The flexible boundary condition approach, in contrast, accounts for the interaction.

Finally, the range of modes of damage should be extended over those of the two-dimensional model to include interply delamination and a "free-edge" effect. The general approach could be similar to that described in References 10 and 11. Attention should first be focused on through-the-thickness cracks in laminated plates under tension with part-through flaws being considered later. Of most importance, the three-dimensional model of an angle ply laminate should permit arbitrarily varied multidirectional layups to be explicitly considered. The properties for the ply moduli could be obtained from laboratory investigations, e.g., in the program being conducted for NASA-Ames at Virginia Polytechnic Institute and State University.

REFERENCES

[1] Mandell, J. F., Wang, S. S., and McGarry, F. J., "The Extension of Crack Tip Damage Zones in Fiber Reinforced Plastic Laminates", J. Composite Mat. 9 (1975) 266.

[2] Sih, G. C. and Liebowitz, H., "Mathematical Theories of Brittle Fracture", Fracture, Vol II, H. Liebovitz, Editor, Academic Press, New York, (1968) p 67.

[3] Gehlen, P. C., Hirth, J. P., Hoagland, R. G., and Kanninen, M. F., "A New Representation of the Strain Field Associated with the Cube-Edge Dislocation in a Model of Alpha-Iron", J. Applied Physics, 42 (1973) 3921.

[4] Kanninen, M. F., "An Analysis of Dynamic Crack Propagation and Arrest for a Material Having a Crack Speed Dependent Fracture Toughness", Prospects of Fracture Mechanics, G. C. Sih, et al, Editors, Noordhoff, Leyden (1974) p 251.

[5] Kanninen, M. F., "A Dynamic Analysis of Unstable Crack Propagation and Arrest in the DCB Test Specimen", Int. J. Fracture, 10 (1974) 415.

[6] Hellen, T. K., "On the Method of Virtual Crack Extension", Int. J. Num. Meth. Eng. 9 (1975) 187.

[7] Hellen, T. K. and Blackburn, W. S., "The Calculation of Stress Intensity Factors for Combined Tensile and Stress Loading", Int. J. Fracture 11 (1975) 605.

[8] Desai, C. S. and Abel, J. F., Introduction to the Finite Element Method, van Nostrand Reinhold Co., New York (1972).

[9] Gaggar, S. and Broutman, L. J., "Crack Growth Resistance of Random Fiber Composites", J. Composite Mat. 9 (1975) 216.

[10] Brinson, H. F. and Yeow, Y. T., "An Investigation of the Failure and Fracture Behavior of Graphite Epoxy Laminates", VPI Report E-75-23, September, 1975.

[11] Rybicki, E. F., "Approximate Three-Dimensional Solutions for Symmetric Laminates Under Inplane Loading", J. Composite Mat. 5 (1971) 354.

[12] Pagano, N. J. and Rybicki, E. F., "On the Significance of Effective Modulus Solutions for Fibrous Composites", J. Composites 8 (1974) 214.

NASA-Langley, 1976